UNIVERSITY OF OVIEDO

SCHOOL OF CHEMISTRY

ORGANOMETALLIC COMPLEXES FOR RECHARGEABLE BATTERIES

(Inorganic Chemistry)

End-of-Degree Project

Irati Ortiz Romero

Oviedo, June, 2023

INDEX

1. ACRONYMS

CES Chemical Energy Storage

CuHCF Copper hexacyanoferrate, of formula $K[CuFe(CN)_6]$

d Doublet, referring to NMR peaks

LIBs Lithium-ion batteries

Li-S Lithium sulphur, referring to batteries

m Multiplet, referring to NMR peaks

MES Mechanical Energy Storage

MOFs Metal Organic Frameworks

Na-S Sodium sulphur, referring to batteries

NMR Nuclear Magnetic Resonance

OA Oxidative Addition

OMCs Organometallic complexes

PB Prussian Blue, of formula $Fe_4[Fe(CN)_6]_3$

PBAs Prussian Blue Analogues

SIBs Sodium Ion Batteries

SMES Superconducting Magnetic Energy Storage

VRB Vanadium Redox Battery

2. ABSTRACT

Organometallic compounds (OMCs) have been gaining importance as materials for the design of batteries relying on their structural diversity, rich porosity, unique charge centres (redox active metals) and relative low price. This work focuses on their use for rechargeable batteries oriented to energy storage, which are indispensable to transition to an energy model based on renewable sources. For this, a bibliographic review of energy storage technologies, focusing on rechargeable batteries and OMCs was carried out. Additionally, three OMCs were chosen to be synthesized and characterized in the laboratory.

3. INTRODUCTION

3.1. Renewable energy and the need for batteries

It is no surprise that the world's energy demand increases day by day, together with the population. The current energy production system relies significantly on fossil fuels (coal, oil, natural gas), which has led to climate change due to an increase of greenhouse gas emissions (**Figure 1**), among other causes. What is more, these energy sources are limited and are now reaching their end, which causes conflicts and prices to skyrocket.[1]

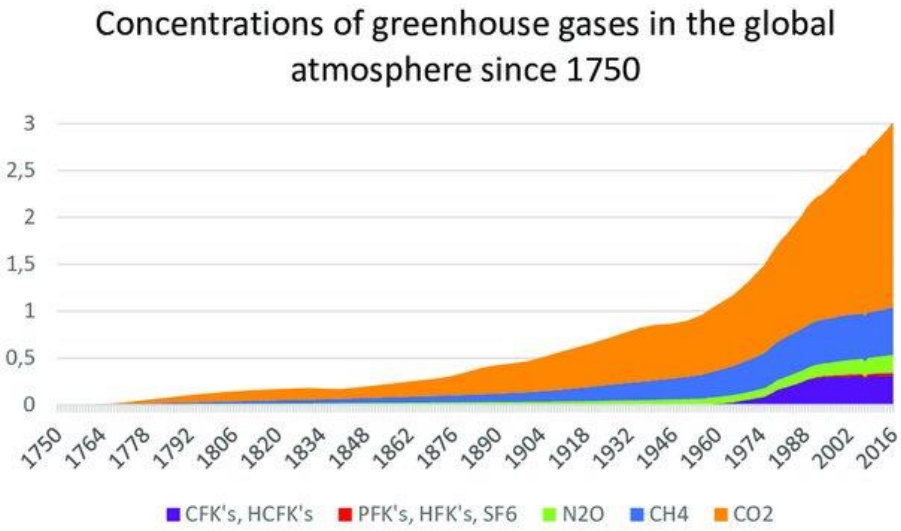

Figure 1. *Concentration of greenhouse gases since 1750, expressed as warming potential.*[2]

Thus, one of the focuses on recent years has been to develop alternative energy sources (renewable energy) trying to mitigate climate change and to ensure that future generations still have energy even when fossil fuels run out.[1]

3.1.1. Renewable energy sources

Renewable energies are defined as energy sources that come from the natural and continuous energy flow that is present on the environment. They are clean sources of

energy, since they produce little waste and help decreasing environmental problems associated to fossil fuels emissions. The main renewable energy sources are wind, solar and ocean energy, hydropower, bioenergy, and geothermal energy.[1]

Wind energy is one of the most used renewable sources. It generates electricity from large turbines from the kinetic energy generated by the movement of these turbines due to the force of the air. Solar energy uses solar irradiation to obtain electricity, using, for example, photovoltaic panels. Ocean energy takes advantage of the energy present in sea areas, such as wind, tides, waves, or thermal difference. Hydropower uses the energy from the movement of water to a lower height (due to gravity) to turn turbines and generate electricity. This is possible using constructions like dams. Bioenergy produces electricity from by-products from forests or agriculture, such as wood waste. Finally, geothermal energy uses the earth's interior heat to generate electricity.[1]

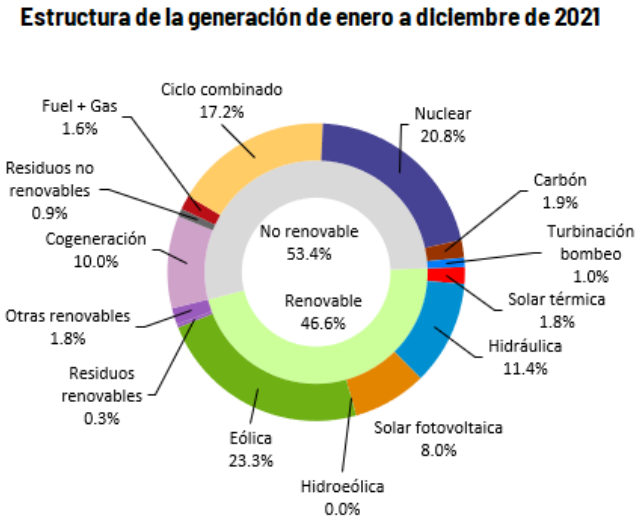

Figure 2. *Energy generation in Spain in 2021. Taken from Red Eléctrica de España.*

This topic can seem quite distant, but these types of energies are already well established in the electricity grid. In Spain (**Figure 2**), almost 47% of the energy generated in 2021 was from renewable energy sources, with 23% being wind energy and 8% being solar energy, making it the second country in Europe in renewable energy production. Hence, the next objective is to make renewable energies the main source of electricity production across the globe.[3] To be able to achieve this, it is important to understand the main limitation of renewable energy sources: lack of consistency, especially wind and solar energies. That is, there are moments in the day where the energy production will be higher than the demand and others where no energy is produced at all. To make this energy sources reliable, the storage of the excess energy must be achieved, so that it can be used when there is a lack

of production due to natural reasons. This introduces the necessity of energy storage technologies.[4]

3.1.2. Energy storage

Energy storage grants the separation of electricity generation from its demand in the energy supply system. This allows the use of intermittent renewable energies (enhancing grid stability and efficiency), which will help achieving a low carbon economy by conserving fossil fuels and reducing their environmental footprint.[4,5] Energy storage technologies can be divided mainly into electrical energy storage (uses electricity produced) and thermal energy storage (uses heat to increase the temperature of a certain mass that can be recovered directly or transformed into electricity by different means when needed). The former will be discussed in this study.[5]

Electrical energy storage systems can be separated at the same time into mechanical, chemical, electrochemical, superconducting magnetic, cryogenic energy storage, etc. depending on the type of energy electricity is converted into.

Mechanical energy storage (MES): it includes systems that convert electrical energy into mechanical energy.

- *Flywheels*: they store energy as rotational kinetic energy in a rotating large mass. During the charge, the electrical energy produced is used to accelerate the motor which spins the mass; for the discharge, the kinetic energy is converted into electrical energy using a generator.[4,5]
- *Pumped hydroelectric storage*: it uses the force of gravity to store energy. Excess electricity is employed to pump water uphill, which is stored in reservoirs. When this energy is needed again, the water is released downhill, which produces electricity by moving hydroturbines.[4,5]
- *Compressed air storage*: this system compresses air using electricity, which is then stored in a reservoir. During discharge, this air is conducted to move a turbine, which generates electricity in the process.[4,5]

Chemical energy storage (CES): it involves systems where electricity is used to form chemical compounds of high energy density, which can be stored to be used when needed. Among the chemicals that can be produced, hydrogen is possibly the most important (what is called green hydrogen if generated using renewable sources). Hydrogen is a high energy density, storable, transportable, versatile, efficient and clean energy carrier; which can be stored as a compressed or liquified gas, in metal hydrides or in organic nanostructures.[6] In its discharge process, hydrogen is either burnt directly or used in fuel cells to produce

electricity. Chemical energy storage has a much higher energy density than mechanical energy storage technologies.[4,5]

Electrochemical energy storage: it includes supercapacitors and batteries.

- *Supercapacitors*: they store energy (by charge accumulation) between each of the two electrodes (that are separated by an electrolyte) and the electrolyte ions (this combination is known as “electric double layer capacitors”). They possess a longer life cycle than batteries but much lower capacities, being very well fitted for short discharge applications.[7]
- *Rechargeable batteries*: they involve (during the charge process) the use of electricity to induce the evolution of a redox reaction inversely to its spontaneous direction, which can be later released (during the discharge process). There are several types, and they can be used for hybrid electric vehicles, portable electronic devices (such as phones or laptops) or wireless network systems, apart from their use as grid energy storage systems.[4,5]

Superconducting magnetic energy storage (SMES): it stores smaller amounts of energy in a superconducting coil, that is at cryogenic temperature (9.8K) to achieve that state. Its main advantage is that it can charge and discharge quickly.[8]

Cryogenic energy storage: the main one is liquid air energy storage (LAES), which stores energy liquifying air (that must be stored in insulated containers) using electricity. In the discharge, the energy from the surroundings is transferred to the liquid air, generating pressure that can be transformed into electricity by mechanical means.[9]

This study focuses on rechargeable batteries as energy storage technologies since they provide many advantages, such as fast response for charge and discharge, wide capacity range, high efficiency, versatility, and wide range of possibilities (depending on the redox reaction used). Additionally, they are compact and operate without producing pollution, making them perfect candidates for the integration of renewable energy sources.[4,5,10,11]

3.2. Rechargeable batteries

A battery is composed of two electrodes; the anode, where an oxidation reaction takes place, and the cathode, where there is a reduction process. Additionally, there is an electrolyte separating them, which forces the electrons out of the battery through an external circuit and at the same time allows the movement of the ions formed during the chemical reactions to maintain the system neutrality. The electrical energy is produced by the work done by the electrons that are forced to move through the circuit from the anode to the cathode. The energy that a battery is capable to release will depend on several factors, such

as the theoretical potential or voltage of the cell (which depends on the reactants used and their form) or the battery internal resistance (which reduces the theoretical voltage and depends on the electrolyte conductivity). For the battery to be rechargeable, both anodic and cathodic reactions must be reversible when applying a charging current and voltage.[12]

There are many types of batteries used for energy storage, and the main ones used for renewable energy storage for the electrical grid system are Lithium-ion, Sodium-sulphur, Lead-acid and flow batteries.

3.2.1. Lithium-Ion Batteries (LIBs)

Li-ion batteries are based on the use of materials that can intercalate lithium either in its metallic form (oxidation state 0) or oxidized form (oxidation state +1). The general construction of a charged LIB consists of an anode (reductor) made of graphite, where metallic Li is stored, and a cathode (oxidant), usually a metal oxide, such as CoO_2, capable of intercalating Li^+ once it is formed during the discharge (Li_xCoO_2 is formed). The electrodes are separated by an electrolyte that allows the migration of lithium ions (Li^+) from the anode to the cathode during the discharge, but is impermeable to the electrons, which are forced to go through the external circuit using metallic collectors made of Cu or Al (**Figure 3**).

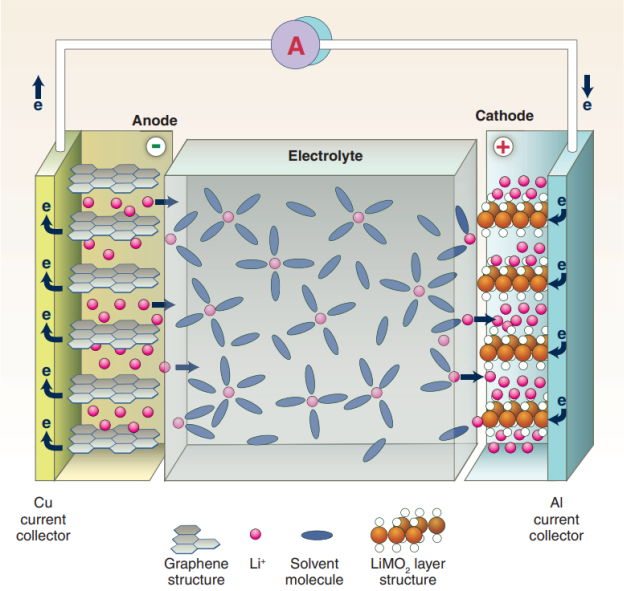

Figure 3. *Representation of a LIB. Obtained from reference 11.*

The first ion battery was constructed by Yoshino, with a carbon anode and a CoO_2 cathode.[12] The reactions taking place are:

$$Li_xC \rightleftharpoons xLi^+ + C + xe^- \text{ (anode)} \quad (1)$$

$$CoO_2 + xLi^+ + xe^- \rightleftharpoons LixCoO_2 \text{ (cathode)} \quad (2)$$

In the discharge process, the Li stored in the graphite layers gets oxidized to Li^+ and passes through the electrolyte to the cathode, where it reacts with the CoO_2 to form the intercalation compound Li_xCoO_2. The electrons produced in the oxidation of Li go through the external circuit from anode to cathode producing electrical energy (note that Co(IV) is reduced to Co(III) per each Li^+ intercalated, accepting the electrons transported by the external circuit). On the other hand, in the charging process, a power source forces the electrons to go back from cathode to anode through the external circuit, causing the oxidation of Co(III) to Co(IV). Consequently, the Li^+ ions leave the Li_xCoO_2 intercalation compound and pass through the electrolyte to the anode, where they get reduced to metallic Li and stored into the graphite layers.

LIBs are leading the portable electronics market and are being considered as the preferred choice for hybrid electric vehicles, and in recent years, they are also being considered for energy storage for the electricity grid. This high demand is due to their outstanding properties, which they owe to the qualities of lithium. Lithium has one of the lowest molecular weights and it possesses a small ionic radius, which helps diffusion during the charging/discharging process. What is more, it has one of the lowest standard reduction potentials ($E^o(Li^+/Li) = -3.04V$), which allows high-output voltages and thus, high energy densities. In addition, LIBs present long cycle life and rate capability (little voltage is lost even at high current loads).[11]

In recent years, these batteries have been improved by controlling properties such as composition, structure or morphology of electrodes and electrolytes.[11] Regarding electrolytes, LIBs commonly use organic liquid electrolytes, such as diethyl carbonates, with a higher voltage limit and good conductivity. However, these electrolytes can be flammable, and alternatives are being explored. Aqueous electrolytes cannot be used since they limit the maximum battery voltage to 1.5V (due to the electrolysis of water) and can also react with metallic lithium in an explosive manner.[12] Regarding the anode, graphite has a limited capacity and, therefore, it is being replaced by materials such as silicon or tin-antimony alloys, where a larger amount of Li can be inserted.[11,12] Another alternative to carbon anodes are organometallic compounds, which will be later discussed. Lastly, for cathodes, the main goal is reducing the costs associated to the use of CoO_2, so alternatives have been studied, such as $LiFePO_4$, which is cheaper and environmentally friendlier; but it is more expensive to maintain and gives lower energy density LIBs.[12]

3.2.2. Sodium-sulphur (Na-S) batteries

They are also known as high-temperature sodium batteries since they use high temperatures to ensure an adequate conductivity for the electrolyte, which is not a liquid at

room temperature. For example, they can use sodium β-alumina ($NaAl_{11}O_{17}$) as a solid electrolyte since β-Alumina is a ceramic refractor material that presents exceptionally high ionic conductivity for Na^+ at high temperatures (around 300ºC). Also, they can use solid inorganic salts, which are guaranteed to be molten at the working temperatures.[11]

Na-S batteries (**Figure 4**) have a sodium anode (which also works as a current collector; negative part) separated by a Na/β-alumina interface from the cathode, which is made of sulphur surrounded by a metallic casing (which works as a current collector; positive part). At the working temperatures both sodium and sulphur are molten. At discharge, Na is oxidized to Na^+ at the Na/β-alumina interface and, at the same time, sulphur is reduced in the cathode to form ionic species that combine with the sodium cations that move through the β-alumina electrolyte to form Na_2S_5 as a final product, which forms a two-phase liquid with sulphur. At charge, the sulphides get oxidized to elemental sulphur, freeing the sodium cations which pass through the interface to go the anode, getting reduced in the process to elemental Na.[5,13]

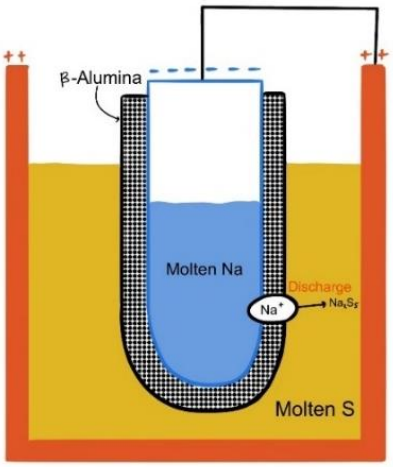

Figure 4. *Representation of a Na-S battery. Derived from reference 5.*

These batteries present many advantages as energy storage candidates for the grid, such as high energy density and efficiency, low maintenance need and long cycle capability. However, they are expensive, require elevated temperatures to operate and the use of metallic sodium can be dangerous, as it is highly reactive.[5]

3.2.3. Redox-Flow batteries

Redox-flow batteries use circulating soluble redox couples stored in separated tanks as electrolytes (catholyte and anolyte) instead of the classical setup of two electrodes and an electrolyte. In between them, there is a selective membrane, which allows the passing of non-reacting ions (e.g., H^+, Na^+), that works as the electrolyte.[11] **Figure 5** shows an example of one of the most advanced flow batteries, the vanadium redox battery (VRB). This

battery is based on the redox reactions of different vanadium ions. During the discharge, the anolyte (containing a V^{2+} source), and the catholyte (containing a V^{5+} source), are pumped from their separate tanks to the reaction chamber, where the selective membrane is, and the redox reaction takes place (V^{2+} is oxidized to V^{3+} and V^{5+} is reduced to V^{4+}). The discharge process enriches the anolyte in V^{3+} and the catholyte in V^{4+}, that can be transformed into the active species, V^{2+} and V^{5+}, during the charge process. The use of only one element presents a great advantage, since the cross-over of vanadium ions through the membrane is less harmful to the battery in the long run.[5,11]

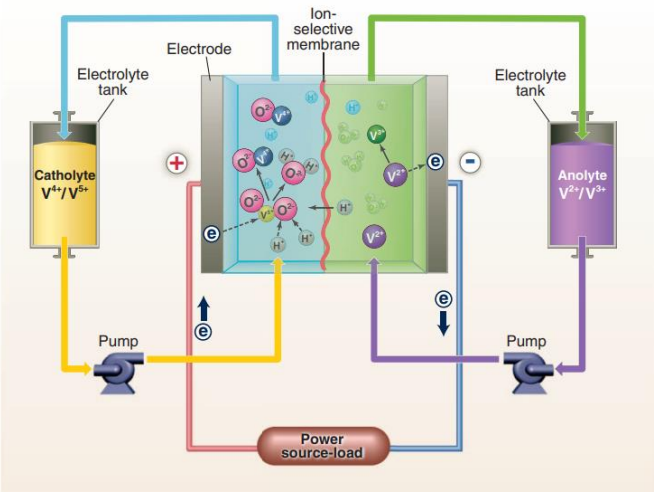

***Figure 5**. Representation of a VRB. Obtained from reference 11.*

The main advantages of redox flow batteries are that they have a low maintenance cost, their electrode reactions are simple, they can achieve high efficiency and energy density, and they can be overcharged or deep charged without affecting the cycle life. Additionally, the separation of the battery active parts, that only produces energy if anolyte and catholyte are pumped to the reaction chamber, ensures a long shelf battery life. However, they require equipment such as pumps, sensors or flow management technology, so they are not ideal for small scale energy storage.[5,11]

3.2.4. Lead Acid batteries

Even though it is the oldest rechargeable battery, it is still in use for some applications (car batteries and small autonomous solar installations) as it presents many advantages such as low maintenance cost, reliability, long battery life and fast response.[5] On the other hand, these batteries have medium-low energy densities (lead is very dense) and present some environmental issues associated with the toxicity of lead. The battery is composed of a PbO_2 cathode and an elemental Pb anode in a concentrated sulphuric acid electrolyte. In the discharge, the Pb^{4+} from the cathode gets reduced to Pb^{2+}, which combines with the

sulphate ions to form $PbSO_4$. At the same time, the Pb from the anode gets oxidized to Pb^{2+}, which also forms $PbSO_4$. This is an example of a comproportionation reaction. During the charge, the $PbSO_4$ disproportionates to regenerate the Pb anode and the PbO_2 cathode.[14]

3.3. Organometallic complexes for rechargeable batteries

The previously discussed batteries are close to reaching their maximum theoretical energy density. Thus, new materials are being studied to overcome the shortcomings of current batteries for energy storage.[15] Organic compounds (carbonyls, organosulphides and radicals) have been considered, since they are cheap and abundant and some of their properties can be easily modified, which allows battery optimization. However, when used as electrode materials (anodes or cathodes) they present some issues related to their solubility and the overall conductivity of the electrolyte. For example, carbonyl compounds have limitations when used as cathodes since the capacity of the battery is reduced due to their high solubility in aprotic solvents (which act as the electrolyte).[15,16]

This is where organometallic complexes (OMCs) come in, because they are composed of metal ions and organic ligands, presenting properties from both groups. They have benefits associated to their high porosity, diverse and adaptable structures (by modification of the organic ligands and the infinite combinations of metal centres possible), they present metal active sites (redox active metals) and they are generally insoluble in the electrolytes used (ensuring no capacity losses). Therefore, OMCs have been proven to have high potential for rechargeable batteries, where they can be used in electrodes or electrolytes.[15] These beneficial properties depend on the structures of the complexes. According to their structure, OMCs can be classified in mainly five groups: metal-organic frameworks (MOFs), porphyrins, phthalocyanines, ferrocene and other complexes.[15]

3.3.1. Metal-organic frameworks (MOFs)

MOFs are organometallic complexes composed of transition metal ions coordinated by multidentate organic ligands with heteroatoms such as O or N. These molecules form a porous periodic crystallin structure, which presents a large surface area and multiple metal centres.[17] These metal ions can go through various valence changes in redox reactions, which provides more electron-storage sites, increasing the battery's capacity (capacity is directly proportional to the number of electrons that can be stored).[18] Their low density and high surface area as well as the possibility of modifying their pore sizes to select the desired power and energy densities make them interesting as electrode materials. What is more, this tunable porosity makes MOFs perfect host materials to produce optimized cathodes for specific oxidants, such as oxygen (small gaseous molecule used in metal-air batteries) or sulphur (large molecular solid used in metal-sulphur batteries). MOFs derivatives are also

being studied for their use as self-supported anodes for LIBs, due to their high mass transport channels, good dispersion, and conductive structure. Additionally, their porosity to filter ions is beneficial, since it avoids the formation of dendrites (lithium accumulation) on the anode.[15,17]

Prussian blue (PB) is a metal organic framework of formula $Fe_4[Fe(CN)_6]_3$ (**Figure 6**), with large interstitial holes, which allows for the mobility of bigger ions such as Na^+. These properties make PB of special interest for Na-ion batteries (SIBs), which have been studied in recent years as alternative to LIBs to harness the high abundance of Na.[19] What is more, it allows for structural modifications, resulting in compounds known as Prussian blue analogues (PBAs). Copper hexacyanoferrate (CuHCF), of formula $K[CuFe(CN)_6]$ for the potassium version (**Figure 7**), is one of them. It can be used as a cathode material that can be operated in aqueous electrolytes, avoiding problems associated to flammable organic electrolytes.[19–21] In this work, both Prussian blue and CuHCF will be synthesized.

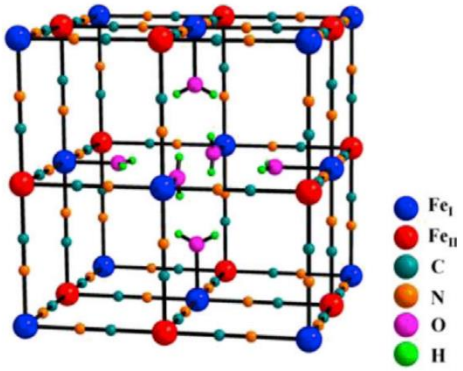

Figure 6. *Prussian blue structure, with lattice water also depicted. Fe_I stands for Fe^{3+} and Fe_{II} for Fe^{2+}. Taken from reference 20.*

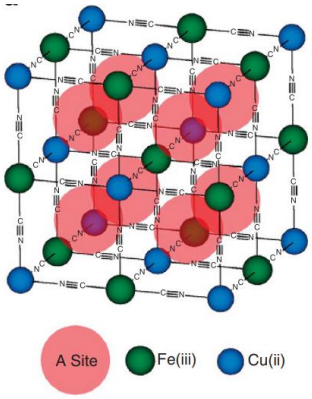

Figure 7*. CuHCF structure. The A sites can be occupied by zeolitic water or cations such as K^+. Taken from reference 21.*

3.3.2. Porphyrin complexes

Porphyrins are heterocyclic macrocycles formed by four pyrrole subunits interconnected with methylene bridges (see **Figure 8a** for a generic representation). They can form complexes with metals where each nitrogen atom, which acts as electron donor, is coordinated to the metal ion (M), which is an electron acceptor. They have been tested in batteries as oxygen electro catalysts for the oxygen reduction reaction in Zn-air batteries, as cathodic materials in metal-ion batteries or as interlayers in Li-S batteries, where they provide cycle stabilization.[15,22]

3.3.3. Phthalocyanine (Pc) complexes

Phthalocyanine is a large heterocyclic compound that forms a macroclycle consisting of four isoindoline units linked by N atoms. It can form complexes with metals such as iron, cobalt, manganese, nickel, or aluminium, which occupy the central cavity (see **Figure 8b** for a generic representation). These compounds present interesting redox properties. They have been tested in batteries as cathode catalysts for the oxygen reduction reaction in Li-air batteries and as cathodic materials for LIBS (since their β-phase presents Li and Na storage properties).[15,23]

3.3.4. Ferrocenes

Ferrocene is an organometallic compound formed by two cyclopentadiene rings coordinated to a central iron ion (see **Figure 8c** for the structure). The latter gives the molecule its redox activity, as it can be oxidized and reduced reversibly. In addition, these reactions are fast, making ferrocene complexes of interest for rechargeable redox flow batteries. It has been studied as a cathode material (for zinc-iodine and LIBs) and as a catholyte for non-aqueous redox flow batteries.[15,24]

3.3.5. Other complexes

In recent years, a broad variety of organometallic complexes have been studied for their use in rechargeable batteries.[15] For example, a report by Mahmoud and coworkers[25], uses several palladium complexes of formula [PdX(4-AcOC$_6$H$_4$)(PPh$_3$)$_2$] (X = Cl, Br, I) (see **Figure 8d**) as components to prepare anode materials for LIBs. They proved to have good cycling stability, high reversibility, and decent specific capacity, which was later improved by controlling the morphology of the particles generated.[25,26] The iodide derivative (X = I) proved to have the best performance (a similar compound to this complex was also chosen to be synthesized in the laboratory).

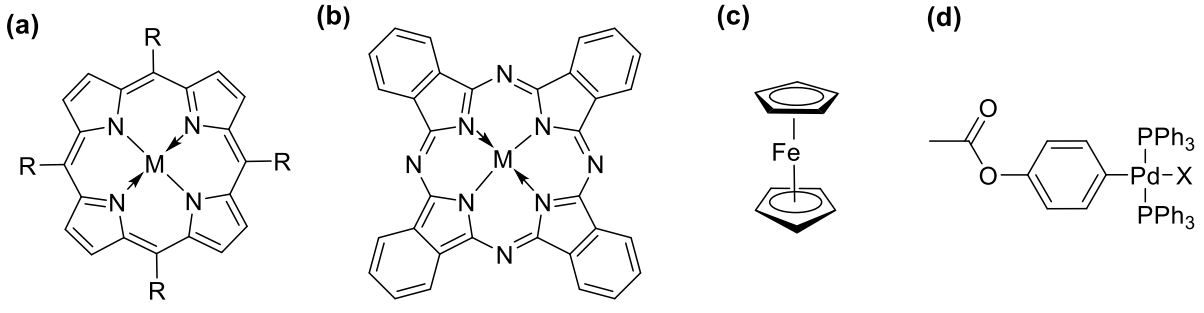

Figure 8. *Some representative examples of organometallic molecular complexes used in batteries.*

4. OBJECTIVES

I. Give an overview on energy storage technologies and their need for implementing intermittent renewable energy sources in the electricity grid, focusing on rechargeable batteries.

II. Review the main rechargeable batteries used for energy storage and how organometallic complexes can be used in their design.

III. Synthesize CuHCF (copper hexacyanoferrate, **A**) and Prussian Blue (**PB**) and characterize them by X-Ray diffraction.

IV. Synthesize [PdI{(C_6H_4)-4-NH_2}(PPh_3)$_2$] (**C**) and characterize it by ^{1}H and ^{31}P NMR. The complex [PdI(4-$AcOC_6H_4$)(PPh_3)$_2$], which has been tested as electrode material in LIBs,[25] could not be synthesized due to the unavailability of 4-iodophenyl acetate.

5. EXPERIMENTAL PART

5.1. General experimental procedures and characterization techniques

All reactions were performed under air, except for the one involving complex **C**, which was done under an inert argon atmosphere using a glove-box and Schlenk-line techniques. All operations were carried out in a well-ventilated fume hood. Lab-coat, safety glasses and protective gloves were worn at all times. All reagents and solvents were purchased from commercial suppliers and used without any further purification, except from hexane and toluene (for the synthesis of **C**), that were dried over sodium and distilled under argon prior to use. Centrifugations were performed on a Selecta Mixtasel BLT. X-Ray diffraction and thermogravimetric analysis were obtained from Servicios Científico Técnicos, Universidad de Oviedo. NMR spectra were run on a Bruker DPX300 instrument; the standards used were the residual protic solvent resonance for ^{1}H [δ($CDCl_3$) = 7.26 ppm] and external 85% H_3PO_4 in D_2O for ^{31}P (δ 0.0 ppm). Section 9.1 of the Supporting Information shows a collection of some photographs taken during the synthesis of the target complexes.

5.2. Labware and other equipment

See Supporting Information (section 9.2)

5.3. Reagents and solvents safety data

See Supporting Information (section 9.3)

5.4. Synthesis and characterization

5.4.1. Synthesis of CuHCF (A)

5.4.1.1. Using a solution of $Cu(NO_3)_2$

Preparation of 50 mL of a 0.1M $Cu(NO_3)_2$ solution

Copper metal (0.51 g), 5 mL HNO_3 0.5M and a stirring magnet were added to a beaker. The mixture was stirred for 10 minutes to remove copper surface impurities (oxides). From that cleaned copper, 0.32 g of the metal (5.0 mmol) were added to a beaker. Then, 5 mL of distilled water, 0.91 mL HNO_3 (65%; 13.3 mmol) and a stirring magnet were added and the mixture was stirred overnight. The next day, a blue solution was obtained with some unreacted metallic copper left. More HNO_3 (65%) was added slowly (9 drops within 2 hours), leading to almost complete copper disappearance. Afterwards, the solution was filtered with a glass funnel and filter paper into a 50 mL volumetric flask, washing the filter with distilled water (the washing was also collected in the volumetric flask, which was filled with more distilled water until a 50 mL volume). The blue solution obtained (50 mL, approximately 0.1M, 5.0 mmol) was used for the next step.

*Preparation of the CuHCF (**A.1**)*

A yellow solution of $K_3[Fe(CN)_6]$ (50 mL, 0.05M, 2.5 mmol) was prepared by dissolving 0.82 g of $K_3[Fe(CN)_6]$ (orange solid) in distilled water in a 50 mL volumetric flask. Two pressure equalizing funnels were attached to a two-necked round bottom flask containing 25 mL of distilled water and a stirring magnet (see Supporting Information for the setup; **Figure S2**). The $Cu(NO_3)_2$ solution was placed on one dropping funnel and the $K_3[Fe(CN)_6]$ one on the other. The solutions were added dropwise simultaneously with constant stirring. A tawny brown precipitate was formed immediately. After the addition was complete, the solution was put into an ultrasonic bath for 20 minutes and the suspension was then allowed to settle overnight (see Supporting Information; **Figure S3**). Afterwards, a filtration using a Büchner funnel by gravity was attempted, but the solid particles were too thin passing through the filter paper (several attempts were done). The separation of the solid from the supernatant solution could be achieved by centrifugation for 5 minutes. Then, the liquid was decanted off and the solid was washed with 80 mL of distilled water, decanting off the washings after a further centrifugation. The remaining slurry was transferred to a beaker and left to dry on top of an oven (30 ºC) overnight. 0.79 g, (100%) of a tawny brown solid, corresponding *a priori* to CuHCF (**A.1**), were obtained (see Supporting Information; **Figure S5**).

Lattice parameter a calculated: 10.1444 Å

Powder X-ray diffraction pattern: See Results and Discussion section.

5.4.1.2. Using solid $Cu(NO_3)_2 \cdot 3H_2O$

Preparation and isolation of $Cu(NO_3)_2 \cdot 3H_2O$

Copper metal (3.2 g, 50.4 mmol) was added to a beaker, along with a stirring magnet, 5 mL of distilled water and 15 mL HNO_3 (65%, 21.9 mmol). The solution was left stirring until the metal was consumed (a large amount of NO_2 evolution was observed, see Supporting Information; **Figure S1**), leading to the formation of a blue solution which was diluted with 10 mL of distilled water. The solution was then filtered (to remove any possible solid particles) with a conical funnel and filter paper, washing with distilled water (the washing was also collected in beaker until reaching a solution volume of approximately 50 mL). Afterwards, the solution was concentrated heating gently with stirring until the volume was reduced to around 15 mL. The concentrated solution was left to cool down at room temperature and was later put into an ice bath briefly, to start the crystallization. The crystalline blue solid obtained was then filtered with a Büchner funnel under vacuum and washed once with 5 mL of cold distilled water. The crystals were left to dry overnight on top of an oven (30 ºC). Solid blue crystals of $Cu(NO_3)_2 \cdot 3H_2O$ (deliquescent solid), wetted by a concentrated $Cu(NO_3)_2$ solution were obtained. Further drying was carried out, first manually with filter paper, and then on a Büchner funnel for 15 minutes under vacuum (0.95 g of $Cu(NO_3)_2 \cdot 3H_2O$, 7.8%). See Supporting Information; **Figure S1**.

*Preparation of the CuHCF (**A.2**)*

A blue solution of $Cu(NO_3)_2$ (50 mL, 0.08M, 4 mmol) was prepared by dissolving 0.95 g of the isolated $Cu(NO_3)_2 \cdot 3H_2O$ (blue solid) in distilled water in a 50 mL volumetric flask. Additionally, a yellow solution of $K_3[Fe(CN)_6]$ (50 mL, 0.05M, 2.5 mmol) was prepared by dissolving 0.83 g of $K_3[Fe(CN)_6]$ (orange solid) in distilled water in another 50 mL volumetric flask. Two pressure equalizing funnels were attached to a two-necked round bottom flask containing 25 mL of distilled water and a stirring magnet (see Supporting Information for the setup; **Figure S2**). The $Cu(NO_3)_2$ solution was placed on one dropping funnel and the $K_3[Fe(CN)_6]$ one on the other. The solutions were added dropwise simultaneously with constant stirring. A tawny brown precipitate was formed immediately. After the addition was complete, the solution was put into an ultrasonic bath for 20 minutes and the suspension was centrifuged for 5 minutes. Then, the supernatant liquid was decanted off and the solid was washed with 80 mL of distilled water, decanting off the washings after a further centrifugation. The remaining slurry was transferred to a beaker and left to dry on top of an oven (30 ºC) overnight. 0.95 g (121%) of a tawny brown solid, corresponding *a priori* to CuHCF (**A.2**), were obtained (see Supporting Information; **Figure S5**).

Lattice parameter a calculated: 10.1510 Å

Powder X-ray diffraction pattern: See Results and Discussion section.

5.4.2. Synthesis of Prussian Blue (PB)

An orange solution of $Fe(NO_3)_3$ (50 mL, 0.01M, 5 mmol) was prepared by dissolving 2.03 g of $Fe(NO_3)_3 \cdot 9H_2O$ (light purple) in distilled water in a 50 mL volumetric flask. Additionally, a light yellow solution of $K_4[Fe(CN)_6]$ (50 mL, 0.05M, 2.5 mmol) is prepared by dissolving 1.04 g of $K_4[Fe(CN)_6] \cdot 3H_2O$ (light yellow) in distilled water in another 50 mL volumetric flask. Two pressure equalizing funnels were attached to a two-necked round bottom flask containing 25 mL of distilled water and a stirring magnet (see Supporting Information for the setup; **Figure S2**). The $Fe(NO_3)_2$ solution was placed on one dropping funnel and the $K_4[Fe(CN)_6]$ one on the other. The solutions were added dropwise simultaneously with constant stirring. A dark blue precipitate was formed instantly. After the addition was complete, the solution was put into an ultrasound bath for 20 minutes and the suspension was then allowed to settle overnight (see Supporting Information; **Figure S3**). Afterwards, the precipitate was filtered slowly with a Büchner funnel under low vacuum. The solid particles were relatively thin and some solid passed through the filter, requiring several filtrations of the collected filtrate. Then, the solid was washed twice with 2 x 10 mL of distilled water and dried in vacuum at room temperature. Finally, the dark blue solid obtained was moved to a watch glass and left to dry on top of an oven at 30ºC overnight. 0.91 g (129%) of a dark blue solid, corresponding *a priori* to Prussian Blue (**PB**) were obtained (see Supporting Information; **Figure S5**).

Lattice parameter a calculated: 10.1675 Å

Powder X-ray diffraction pattern: See Results and Discussion section.

5.4.3. Synthesis of $[PdI\{(C_6H_4)\text{-}4\text{-}NH_2\}(PPh_3)_2]$ (C)

Under an inert argon atmosphere in a glove box, 49.4 mg of $[Pd(PPh_3)_4]$ (0.043 mmol) and 10.8 mg 4-iodoaniline (0.049 mmol) were added to a 50 mL Schlenk containing a stirring magnet. Then, 3 mL of dry toluene were added, resulting in a yellow suspension which was stirred at room temperature for 1 h (see Supporting Information; **Figure S4**). An aliquot of the reaction crude was taken and analysed by ^{1}H and ^{31}P NMR (see Supporting Information; **Figures S9** and **s10**). The $^{31}P\{^{1}H\}$ NMR spectrum showed, among other signals, a singlet at 22.7 ppm, different to that corresponding to $[Pd(PPh_3)_4]$, which was not present (see Supporting Information; **Figure S8**). Outside of the glove box, using Schlenk-line techniques, 7 mL of dry hexane were added to induce further precipitation of a light-yellow solid (see

Supporting Information; **Figure S4**). Then, the supernatant solution was decanted off and the solid was washed with 10 mL of more dry hexane, which was also decanted. The resulting light-yellow powder was left to dry in vacuum for 3 hours. 36 mg (99%) of a light-yellow solid were obtained, corresponding to compound **C** partially impurified with other species (in respect to this, see Results and Discussion section). The data shown below corresponds only to signals of **C**.

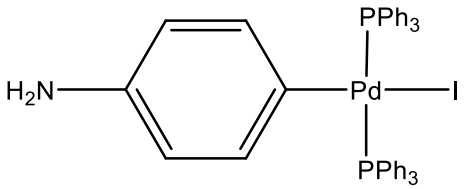

[PdI{(C_6H_4)-4-NH_2}(PPh_3)$_2$] (**C**)

^{1}H-NMR (300.1 MHz, 298 K, $CDCl_3$, ppm): 7.60–7.47 and 7.40-7.25 (m, 30H, 6 Ph), 6.27 (d, J = 8.25 Hz, 2 H, 2 CH *meta* to NH_2), 5.80 (d, J = 8.25 Hz, 2H, 2 CH *ortho* to NH_2), 3.00 (br, 2H of NH_2).

^{31}P-NMR (121.5 MHz, 298 K, $CDCl_3$, ppm): 22.7 (s).

6. RESULTS AND DISCUSSION

6.1. CuHCF (A)

Commercial $Cu(NO_3)_2{\cdot}3H_2O$ was not available by the time the laboratory started, so the $Cu(NO_3)_2$ solution needed for the preparation of CuHCF was prepared directly from metallic copper and HNO_3 (synthesis of CuHCF (**A.1**)). Having in mind the possibility that a certain amount of acid could also be present in this solution, affecting the reaction outcome, isolated $Cu(NO_3)_2{\cdot}3H_2O$ (prepared in the laboratory) was also used for the synthesis of CuHCF (**A.2**).

6.1.1. Reactions

Synthesis of copper nitrate

According to the literature, the reaction of metallic copper and HNO_3 can occur through two possible reactions (see equations 3 and 4).[27] Both are redox reactions, where Cu gets oxidized to Cu^{2+} by HNO_3, which is reduced to either NO_2 or NO (NO can also get oxidized to NO_2 by molecular oxygen). Reaction 4 is favoured at low temperature and using dilute acid, while reaction 3 occurs when concentrated HNO_3 is used. For the direct synthesis,

aiming at minimizing any possible excess of acid, the needed amount of copper (for the 50 mL of the 0.1M solution required) was reacted with a 0.5M HNO_3 solution. This reaction proved to be very slow and did not consume all copper after overnight stirring. To consume all remaining copper, concentrated HNO_3 was added dropwise (9 drops in 2 hours) until essentially no more copper was left (using concentrated HNO_3 a brown gas was seen when performing the reaction, which corresponds to NO_2, since NO is colourless). In this way, the needed amount of $Cu(NO_3)_2$ to prepare the required 0.1M solution was obtained.

$$Cu + 4HNO_3 \rightarrow Cu(NO_3)_2 + 2H_2O + 2NO_2 \quad (3)$$

$$3Cu + 8HNO_3 \rightarrow 3Cu(NO_3)_2 + 4H_2O + 2NO \quad (4)$$

$Cu(NO_3)_2 \cdot 3H_2O$ was isolated concentrating a $Cu(NO_3)_2$ solution (quickly prepared from Cu and concentrated HNO_3). The compound is very soluble in water, so the crystallization was very difficult.[27] After some attempts, the compound was finally crystalized, however, when washing the solid with cold water to remove the excess nitric acid present, a large amount of the solid was dissolved and lost. Thus, the yield for the process was only 8%. Despite this, enough solid was obtained to have an excess of this reagent in the following reaction, so it could be carried out as planned.

Synthesis of copper hexacyanoferrate

$$Cu(NO_3)_2 + K_3[Fe(CN)_6] \rightarrow K[CuFe(CN)_6] \downarrow + 2KNO_3 \quad (5)$$

The reaction (equation 5) between $Cu(NO_3)_2$ and $K_3[Fe(CN)_6]$ is a double replacement reaction, where the anions and cations of the reagents are exchanged driven by the formation of a precipitate, that is CuHCF, and a salt that remains dissolved (KNO_3). The reaction is 1:1, but it was performed with a 2:1 ratio (excess of $Cu(NO_3)_2$), since the presence of excess Cu^{2+} slows down the coprecipitation of the solid, according to the literature.[21] However, in both cases (using the two sources described for $Cu(NO_3)_2$), the particles obtained experimentally were very fine, to the point where centrifugation was needed to isolate the product (filtration was not effective as described in the experimental part). CuHCF was prepared following the procedure reported by Wessells and co-workers.[21]

6.1.2. Structure

CuHCF is a Prussian Blue analogue and presents the usual open-framework PB structure, which is analogous to ABX_3 perovskites (see **Figure 9**). In the case of CuHCF (**Figure 10**),

the Cu^{2+} and Fe^{3+} ions define a cubic unit cell in an alternating manner (B ions), the K^+ ions occupy the A sites in the centre, and the CN^-, corresponding to X, surround the B ions in an octahedral manner (note that the CN^- are bridging Cu^{2+} and Fe^{3+} cations in a way the N atoms are bound to Cu^{2+} and the C atoms to Fe^{3+}).[21] The crystalline structure can also be described as alternating FeC_6 and CuN_6 octahedra, that are connected by short C-N bonds, resulting in a cubic open framework.[20]

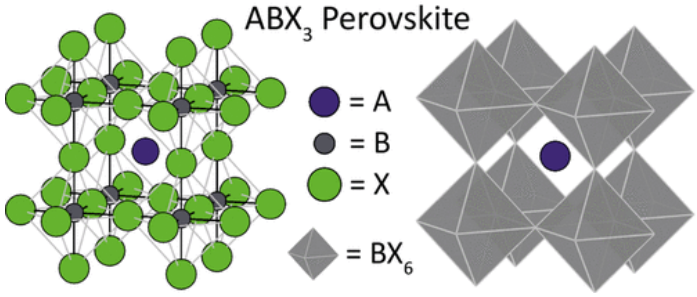

***Figure 9**. Structure of ABX_3 perovskites, depicted with all the atoms (left) and only the BX_6 octahedra (right).*[28]

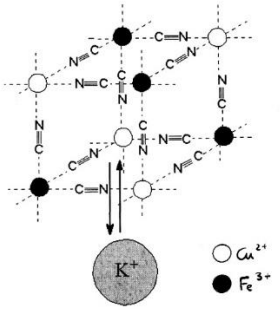

***Figure 10.** CuHCF structure (the unit cell is made of 8 of these cubic structures).*[29]

6.1.3. Characterization

Characterization of CuHCF

Both solids **A.1** and **A.2** were characterized by powder X-Ray diffraction, which showed that the materials have a good crystallinity (see diffraction patterns in **Figure 11** and **Figure 12**).

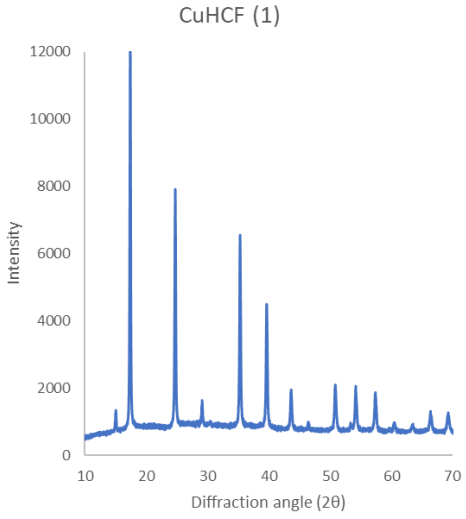

***Figure 11.** Diffraction pattern obtained for compound **A.1**.*

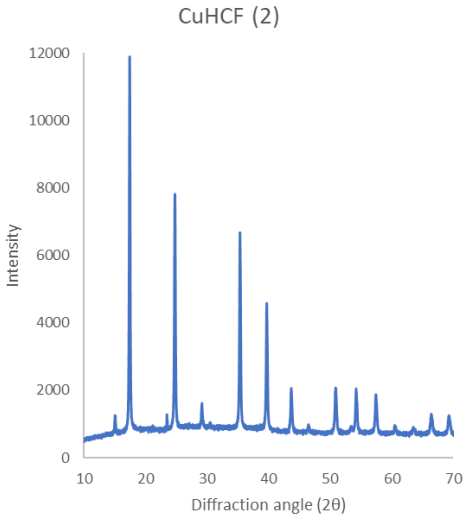

***Figure 12.** Diffraction pattern obtained for compound **A.2**.*

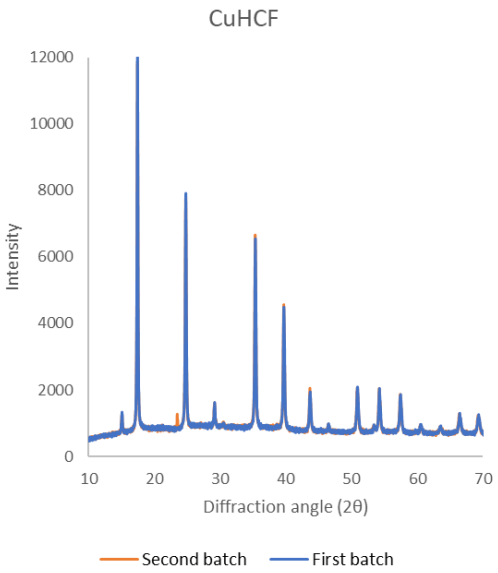

Figure 13. *Combined diffraction patterns of compound* ***A.1*** *(blue) and* ***A.2*** *(orange).*

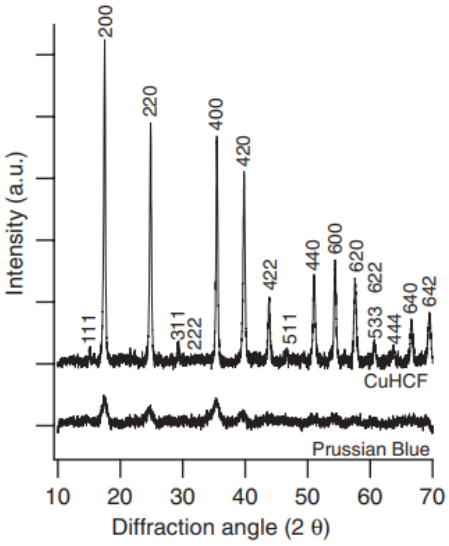

Figure 14. *Diffraction patterns reported for CuHCF (top) and Prussian Blue (bottom). Taken from reference 21.*

The diffraction patterns obtained for both procedures were almost identical (see **Figure 13** for an overlap view), indicating that both methods (using a $Cu(NO_3)_2$ solution synthesized directly or the isolated $Cu(NO_3)_2 \cdot 3H_2O$ as reagent) yielded the same structure. Also, the pattern obtained is essentially the same as that reported in the literature for CuHCF (**Figure 14**).[21] As explained above, CuHCF presents a cubic structure, so it possesses a single lattice parameter (*a*) which was calculated from the experimental data. For **A.1**, *a* has a value of 10.1444 Å, while for **A.2**, *a* is 10.1510 Å. Both values are very close to each other and to the one found in the literature, which is 10.1397 Å.[30] This is another proof that the products present the expected structure.

Characterization of $Cu(NO_3)_2 \cdot 3H_2O$

The literature reports that $Cu(NO_3)_2$ can crystalize as $Cu(NO_3)_2 \cdot 3H_2O$ or $Cu(NO_3)_2 \cdot 6H_2O$.[27] A thermogravimetric analysis (TG-DTG-SDTA and TG-MS) was performed with the crystalline $Cu(NO_3)_2$ prepared. The sample was concluded to be trihydrated after performing mass loss calculations (this analysis of the data was carried out by the Servicios Científico-Técnicos, Universidad de Oviedo).

6.1.4. Yield

Assuming **A.1** and **A.2** were obtained as pure products, the isolation yields were 100 % (0.79 g) and 121 % (0.95 g), respectively. In both cases, the weight was measured after assuring that there was no weight change of the isolated solids, which were left to dry on top of an oven at 30ºC, in at least one day. The very high (for **A.1**) or impossible (for **A.2**) values obtained are possibly due to: (i) both solids still have residual humidity that needs higher temperature to get removed and/or (ii) both solids are impurified with a certain amount of the reaction side products (KNO_3 formed and $Cu(NO_3)_2$ used in excess) due to lack of washing. KNO_3 being an impurity is more probable than $Cu(NO_3)_2$, since the latter has a much higher solubility. The reference paper followed[21] does not provide any yield so it cannot be compared.

6.2. Prussian Blue (PB)

This compound of formula $Fe_4[Fe(CN)_6]_3$ (**PB**), named Prussian Blue, was synthesized to compare its structural data with that of CuHCF (**A**), which is a PB analogue. The procedure reported by Wessells and co-workers was followed.[21]

6.2.1. Reaction characteristics

$$4Fe(NO_3)_3 + 3K_4[Fe(CN)_6] \rightarrow Fe_4[Fe(CN)_6]_3 \cdot nH_2O\downarrow + 12KNO_3 \quad (6)$$

The reaction (equation 6) between $Fe(NO_3)_3$ and $K_4[Fe(CN)_6]$ is the same as that involving the formation of CuHCF; a double replacement reaction driven by the formation of a precipitate, that is the Prussian blue, while KNO_3 remains dissolved. The reaction was performed with a 2:1 excess of $Fe(NO_3)_3$, since the presence of excess Fe^{3+} allows the formation of the desired compound, which is also known as “insoluble” Prussian Blue ($Fe_4[Fe(CN)_6]_3 \cdot nH_2O$), that includes hydration water molecules in its formula. If the reaction was performed stoichiometrically, K^+ ions would be incorporated into the crystal structure, resulting in what is known as “soluble” Prussian Blue ($KFe[Fe(CN)_6] \cdot nH_2O$).[31] The precipitation was instantaneous, resulting in a very fine dark blue powder. Nevertheless, this solid, differently to CuHCF, could be filtrated with a Büchner filter without the need of centrifugation (see experimental part for more details).

6.2.2. Structure

The “insoluble” Prussian Blue, of formula $Fe_4[Fe(CN)_6]_3 \cdot nH_2O$ has a structure analogous to ABX_3 perovskites, as stated above, but shows important differences. The Fe^{2+} and Fe^{3+} ions occupy the corners of a cube in an alternating manner (B ions), however, a vacancy of an Fe^{2+} cation is found in one of the corners. No ions occupy the A sites in the centre (as in CuHCF), and the CN^- corresponding to X, surround most of the B ions in an octahedral manner (note that the CN^- are bridging Fe^{2+} and Fe^3 anions in a way the N atoms are bound to Fe^{3+} and the C atoms to Fe^{2+}). **Figure 15** shows the unit cell of “insoluble” Prussian Blue, formed by 8 $Fe^{III}_4Fe^{II}_3$ cubes sharing its $[Fe(CN)_6]^{4-}$ vacancy, which lies in the center. H_2O molecules are bound to some of the ions that, due to the vacancy mentioned, are only surrounded by 5 CN^- ligands. The absence of these vacancies in PBAs, as in the case of CuHCF, makes them present better crystallinity than PB and thus, better properties as energy storage compounds.[20,31]

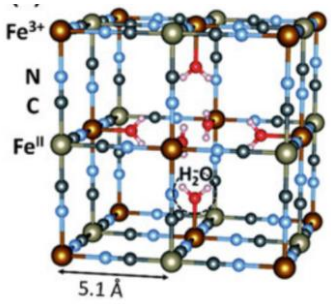

Figure 15. *"Insoluble" Prussian Blue unit cell ($Fe_4[Fe(CN)_6]_3 \cdot nH_2O$. Taken from reference 31.*

6.2.3. Characterization

The solid obtained, which is supposed to be “insoluble” Prussian Blue ($Fe_4[Fe(CN)_6]_3 \cdot nH_2O$), was characterized by powder X-Ray diffraction (its diffraction pattern is shown in **Figure 16**. It is clear that the compound presents poor crystallinity, especially when compared to CuHCF, with significantly lower intensity peaks. This diffraction pattern is very similar to that found for the same compound in the literature (**Figure 17**). [21]

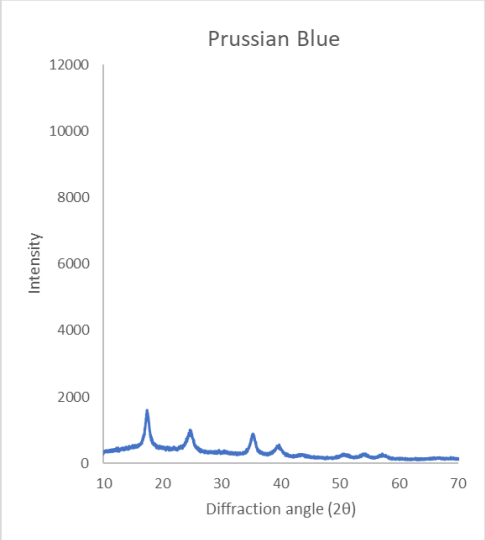

***Figure 16**. Diffraction pattern obtained for Prussian Blue (**PB**).*

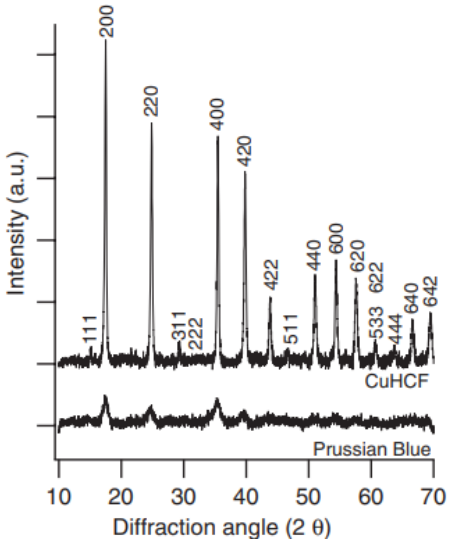

***Figure 17.** Diffraction patterns reported for CuHCF (top) and Prussian Blue (bottom). Taken from reference 21.*

The lattice parameter was also calculated for the Prussian Blue synthesized (**PB**), having a value for *a* of 10.1675 Å, which is very close to the value reported on the literature, 10.178 Å.[31] Thus, it can be concluded that despite not presenting great crystallinity, the compound synthesized is Prussian Blue. Also, this parameter can be compared to those of CuHCF, which are 10.1444 Å (for **A.1**) and 10.1510 Å (for **A.2**). It is clear that the values are quite close, which is expected since CuHCF is a PBA also featuring CN^- ligands.

6.2.4. Yield

Assuming that **PB** was obtained as a pure product, the isolation yield was 129 % (0.91 g). The weight was measured after assuring that there was no weight change of the solid isolated in at least one day, which was left to dry on top of an oven (30 ºC). The impossible value of yield obtained is possibly due to two reasons. Firstly, the yield was calculated for a compound of formula $Fe_4[Fe(CN)_6]_3$, when the obtained solid, "insoluble" PB, possesses water molecules that are part of the crystalline structure ($Fe_4[Fe(CN)_6]_3 \cdot nH_2O$). Thus, the real molecular weight of the solid, which is not accurately known, is certainly higher that the value used for the calculation (a higher molecular weight would give a lower yield). Secondly, insufficient washing can also contribute to the high yield. The reaction side products are KNO_3 which, as stated above, is moderately soluble in cold water, and $Fe(NO_3)_3$ used in excess, which is very soluble. Therefore, KNO_3 being an impurity is more probable. The reference paper followed[21] does not provide any yield so it cannot be compared.

6.3. [PdI{(C_6H_4)-4-NH_2}$(PPh_3)_2$] (C)

Complex **C** was synthesized instead of [PdI(4-$AcOC_6H_4$)$(PPh_3)_2$], a Pd complex that has been tested as electrode material in LIBs,[25] since as previously mentioned, 4-iodophenyl acetate was not available by the time the laboratory started. However, since the structure of complex **C** is very similar, only differing in the substituent of the aryl ligand, it would be expected that **C** would also have good properties as electrode material in LIBs.

6.3.1. Reaction characteristics

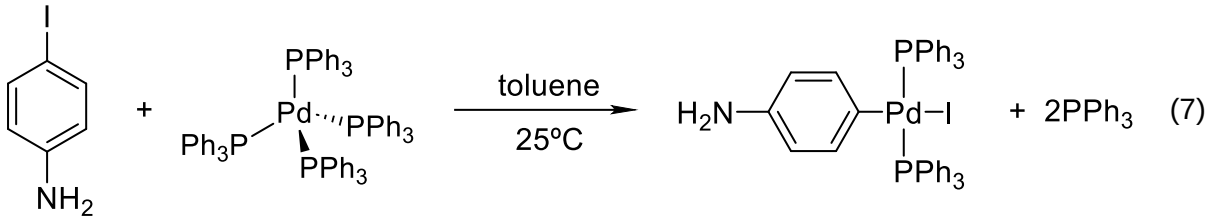

(7)

Complex **C** was prepared following a similar procedure to that reported for the preparation of [PdI(4-$AcOC_6H_4$)$(PPh_3)_2$], [25] reacting 4-iodoaniline with [$Pd(PPh_3)_4$] in a 1:1 ratio in toluene at room temperature (see experimental part). This reaction (equation 7) can be described as the result of an oxidative addition (OA) to Pd(0), since upon the C–I bond cleavage of 4-iodoaniline, a Pd(II) species is formed (complex **C**) featuring, in addition to two PPh_3 neutral ligands, two anionic ligands (aryl and iodide).

[$Pd(PPh_3)_4$] is a tetrahedral d^{10} complex, with 18 electrons and therefore, in order to incorporate the new two ligands, coordination vacancies must be generated, for example by losing one or more PPh_3 ligands.[32,33] It is reported that this kind of reactions can follow a mechanism (see **Figure 18**) where the Pd(0) unsaturated species interacts with the aryl C_{sp2}–I bond promoting its cleavage by donating electron density to its σ* orbital via a concerted (or three-centre) transition state.[33] Therefore, these reactions are favoured for electron rich metals in low oxidation states and surrounded by donor ligands, such as the Pd(0) complex used.[33] Another important consideration is that, assuming the concerted mechanism is followed, the *cis* isomer should be the initial reaction product. However, it is commonly observed that the *cis* isomer spontaneously undergoes isomerization to form the *trans* isomer, more stable thermodynamically due to sterical constraints.[34]

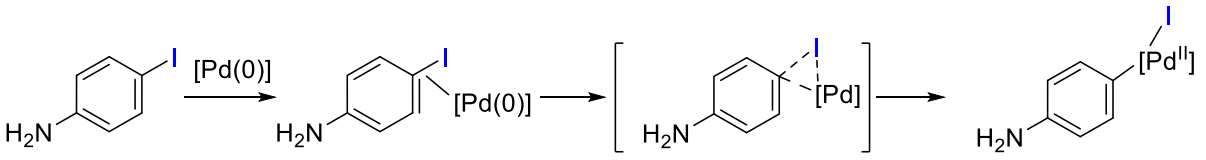

Figure 18. *Schematic representation of an oxidative addition of 4-iodoaniline to a Pd(0) complex. The Pd complex is simplified without including other ligands.*

6.3.2. Structure

The final complex has a square planar structure (related compounds have the same coordination geometry)[35] with two possible isomers, the *cis* one, where the PPh_3 ligands are next to each other (**Figure 19**), and the *trans* isomer, where they are opposite to each other (**Figure 20**). The Figures show clearly that the *cis* isomer has a lower stability than the *trans*, since the phenyl groups of the PPh_3 ligands of the former are much closer to each other, causing steric hindrance. Thus, the isomerization mentioned is reasonable.

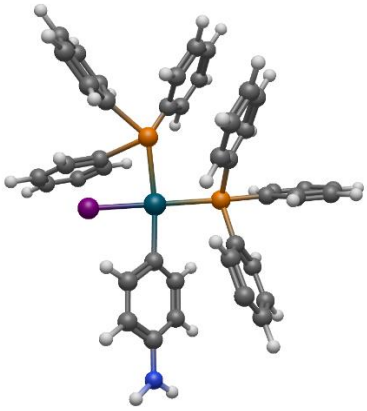

Figure 19. *3D Representation of the cis isomer of the Pd complex (**C**). Depicted with Avogadro2.*

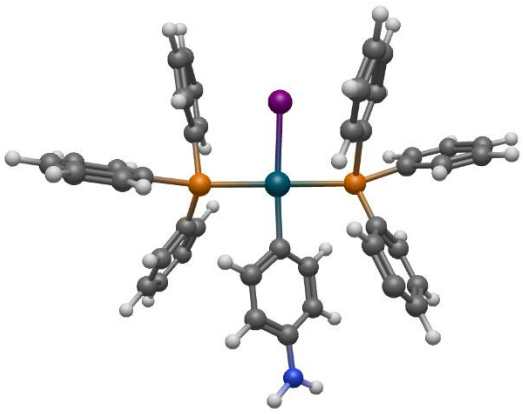

Figure 20. *3D Representation of the trans isomer of the Pd complex (**C**). Depicted with Avogadro2.*

6.3.3. Reaction evolution and product characterization

The evolution of the reaction was checked by ^{1}H and ^{31}P NMR (see experimental part and Supporting Information; section 9.4), showing reaction completion after 1 h since: (i) a signal at –5.1 ppm, corresponding to free PPh_3, is observed, (ii) another signal of similar intensity at 22.7 ppm is observed, which can be assumed to correspond to the desired product **C**, (iii) there is no signal corresponding to the starting material $[Pd(PPh_3)_4]$, which shows a singlet at 28 ppm, and (iv) the signals corresponding to the (C_6H_4)-4-NH_2 unit are very different from those of 4-iododaniline. The $^{31}P\{^{1}H\}$ NMR spectrum also shows a minor peak at 33.5 ppm of unknown identity. Complex **C** was reported by Vicente et al.,[35] showing on its ^{31}P NMR also a singlet at 22.7 ppm, which confirms its successful formation in our case as a major product. Additionally, the unique signal observed is in agreement with the *trans* configuration proposed, since a *cis* isomer would give two doublets.

The reaction crude was washed with hexane (to remove the PPh_3 released) yielding 36 mg of a light-yellow powder. A $^{31}P\{^{1}H\}$ of this solid (**Figure 21**) shows that the signal of free PPh_3 does not appear, so it can be concluded that the washings were performed correctly. However, in addition to the signal of complex **C** at 22.7 ppm, more signals appear, particularly one at 23.2 ppm. The nature of these other signals is unknown. Overall, after the

isolation process, complex **C**, which was formed as a major product in the reaction, suffered further evolution to other products and, although was isolated as a major compound, was not isolated pure. It should be noted that all operations were carried out under argon atmosphere.

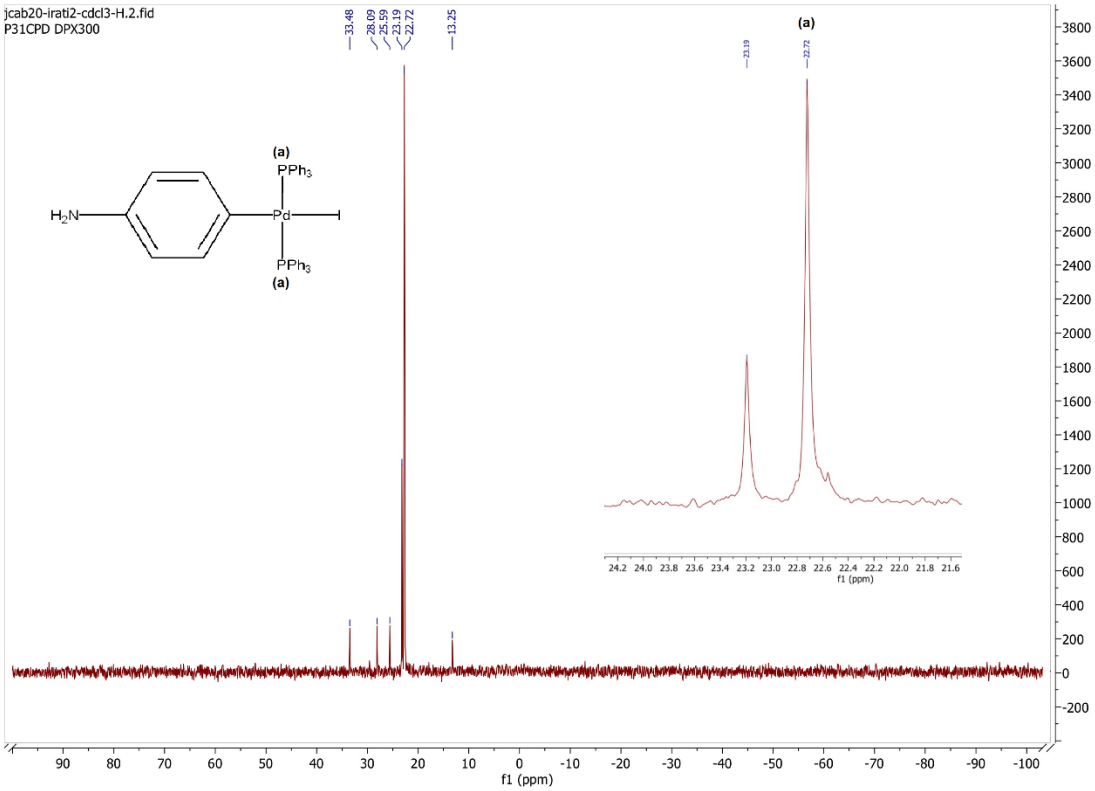

Figure 21. *$^{31}P\{^{1}H\}$ NMR spectrum of the isolated reaction product. It includes a close-up of the stronger peaks on the right.*

A ^{1}H NMR spectrum was also carried out and further aided in the characterization of the complex (**Figure 22**). The existence of a mixture makes the identification of the signals corresponding to **C** problematic, however a set of signals, mixed with other minor ones, corresponding the Ph groups of the PPh_3 ligands, to the CHs of the aryl group (2 Hb and 2 Hc) and to the NH_2 group of **C** can be observed at similar chemical shifts than the values reported for Vicente et al.[35]

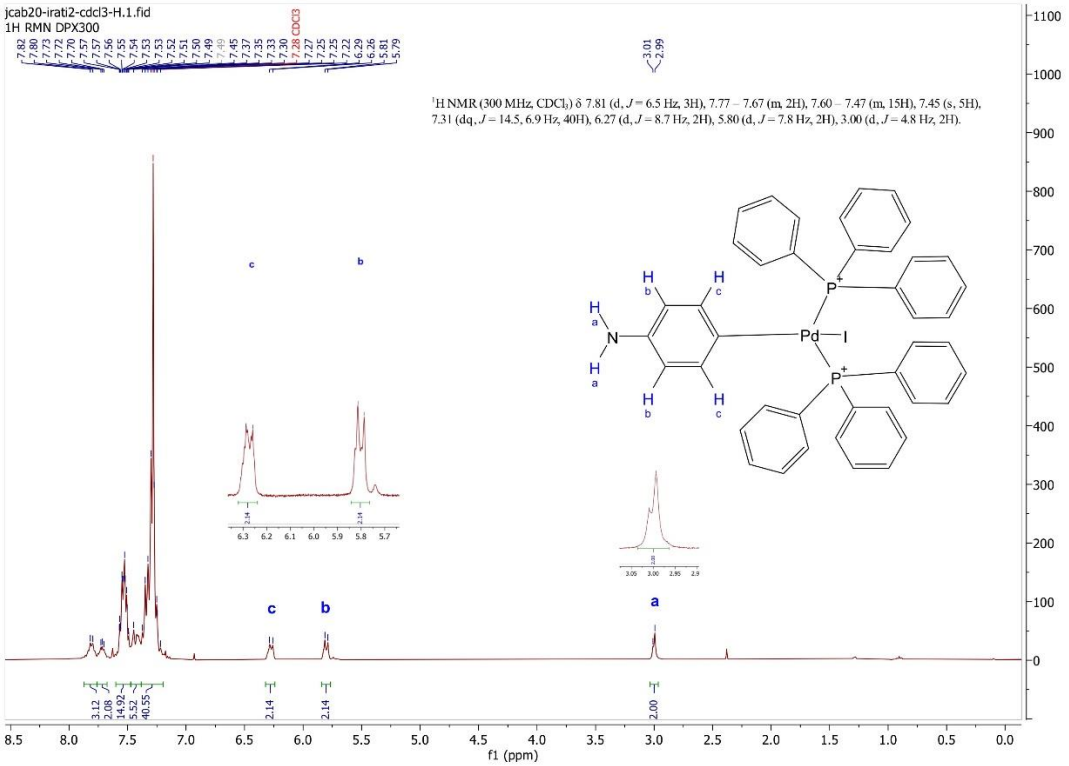

***Figure 22**.[1]H NMR spectrum of the isolated reaction product. It includes a close-up of the peaks corresponding to the a,b and c hydrogens.*

6.3.4. Yield

The yield obtained for the product, assuming it was pure, would be of 99%. However, according to the data provided by NMR, this yield is lower. The paper by Vicente et al.[35] reports a 78 % isolation yield, nevertheless, they used a different method for the preparation of **C** and a direct comparison cannot be done.

7. CONCLUSIONS

-The importance of organometallic complexes due to their unique properties for the construction of rechargeable batteries intended for renewable energy storage is a topic of current research.

-Complexes from two of the main types of OMCs: metallic organic frameworks (CuHCF (**A**) and Prussian Blue (**PB**)) and Pd complexes (in particular $[PdI\{(C_6H_4)\text{-}4\text{-}NH_2\}(PPh_3)_2]$ (**C**)) were synthesized in the laboratory.

-CuHCF (**A**) and Prussian Blue (**PB**) were prepared successfully according to characterization data obtained (Powder X-ray diffraction), however the very high or

impossible yields obtained point to the existence of some impurities in the isolated products (further washing might solve this problem).

-Centrifugation is a better method (less time consuming) for the isolation of both CuHCF (**A**) and Prussian Blue (**PB**), since they form solids with a very small particle size difficult to isolate by filtration.

-There was no apparent difference in the structure of CuHCF when using a $Cu(NO_3)_2$ solution synthesized directly or the isolated $Cu(NO_3)_2 \cdot 3H_2O$ as reagent.

-$[PdI\{(C_6H_4)\text{-}4\text{-}NH_2\}(PPh_3)_2]$ (**C**) was isolated and characterized, although some impurities (possibly due to product instability and evolution to other species) were present in the final product, which was proven to be the *trans* isomer.

8. BIBLIOGRAPHY

1. Owusu PA, Asumadu-Sarkodie S. A review of renewable energy sources, sustainability issues and climate change mitigation. *Cogent Eng*. **2016**, 3(1), 1167990-1168003. DOI:10.1080/23311916.2016.1167990
2. Van Ackere S. Flood Impact Assessment Tool (FLIAT) - An Object-Relational GIS Tool for Impact Assessment in Flanders, Belgium. Ph.D. Thesis, Ghent University, November 2019. DOI:10.13140/RG.2.2.10170.75203
3. Webpage (see at the end).
4. Carrasco JM, Franquelo LG, Bialasiewicz JT, et al. Power-electronic systems for the grid integration of renewable energy sources: A survey. *IEEE T Ind Electron*. **2006**, 53(4), 1002-1016. DOI:10.1109/TIE.2006.878356
5. Aneke M, Wang M. Energy storage technologies and real life applications – A state of the art review. *Appl Energy*. **2016**, 179, 350-377. DOI:10.1016/j.apenergy.2016.06.097
6. Von Jouanne A, Husain I, Wallace A, Yokochi A. Innovative hydrogen/fuel cell electric vehicle infrastructure based on wind energy sources. *38th IAS Annual Meeting on Conference Record of the Industry Applications Conference*, Salt Lake City, UT, USA, **2003**, 2, 716-722. DOI:10.1109/IAS.2003.1257598
7. Tan X, Li Q, Wang H. Advances and trends of energy storage technology in Microgrid. *Int J Elect Power*. **2013**, 44(1), 179-191. DOI:10.1016/j.ijepes.2012.07.015
8. Erik Nielsen K, Molinas M. Superconducting Magnetic Energy Storage (SMES) in Power Systems with Renewable Energy Sources. *2010 IEEE International Symposium on Industrial Electronics*, Bari, Italy, **2010**, 2487-2492 DOI:10.1109/ISIE.2010.5637892

9. Ding Y, Tong L, Zhang P, Li Y, Radcliffe J, Wang L. Liquid Air Energy Storage. *Storing Energy: With Special Reference to Renewable Energy Sources*. Elsevier Inc.; **2016**, 167-181. DOI:10.1016/B978-0-12-803440-8.00009-9
10. Larcher D, Tarascon JM. Towards greener and more sustainable batteries for electrical energy storage. *Nat Chem*. **2015**, 7(1), 19-29. DOI:10.1038/nchem.2085
11. Dunn B, Kamath H, Tarascon JM. Electrical Energy Storage for the Grid: A Battery of Choices System power ratings, module size. *Science*. **2011**, 334, 928-935. DOI:10.1126/science.1212741
12. Goodenough JB, Park KS. The Li-ion rechargeable battery: A perspective. *J Am Chem Soc*. **2013**, 135(4), 1167-1176. DOI:10.1021/ja3091438
13. Wen Z, Cao J, Gu Z, Xu X, Zhang F, Lin Z. Research on sodium sulfur battery for energy storage. *Solid State Ion*. **2008**, 179(27-32), 1697-1701. DOI:10.1016/j.ssi.2008.01.070
14. Jung J, Zhang L, Zhang J. Lead-Acid Battery Technologies: Fundamentals, Materials and Applications (1st ed.), CRC Press, **2015**. DOI:10.1201/b18665
15. Wang DY, Liu R, Guo W, Li G, Fu Y. Recent advances of organometallic complexes for rechargeable batteries. *Coord Chem Rev*. **2021**, 429. DOI:10.1016/j.ccr.2020.213650
16. Lu Y, Chen J. Prospects of organic electrode materials for practical lithium batteries. *Nat Rev Chem*. **2020**, 4(3), 127-142. DOI:10.1038/s41570-020-0160-9
17. Mehtab T, Yasin G, Arif M, et al. Metal-organic frameworks for energy storage devices: Batteries and supercapacitors. *J Energy Storage*. **2019**, 21, 632-646. DOI:10.1016/j.est.2018.12.025
18. Liu C, Neale ZG, Cao G. Understanding electrochemical potentials of cathode materials in rechargeable batteries. *Materials Today*. **2016**, 19(2), 109-123. DOI:10.1016/j.mattod.2015.10.009
19. You Y, Wu XL, Yin YX, Guo YG. High-quality Prussian blue crystals as superior cathode materials for room-temperature sodium-ion batteries. *Energy Environ Sci*. **2014**, 7(5), 1643-1647. DOI:10.1039/c3ee44004d
20. Wang B, Han Y, Wang X, et al. Prussian Blue Analogs for Rechargeable Batteries. *iScience*. **2018**, 3, 110-133. DOI:10.1016/j.isci
21. Wessells CD, Huggins RA, Cui Y. Copper hexacyanoferrate battery electrodes with long cycle life and high power. *Nat Commun*. **2011**, 2(1). DOI:10.1038/ncomms1563
22. Li BQ, Zhang SY, Wang B, Xia ZJ, Tang C, Zhang Q. A porphyrin covalent organic framework cathode for flexible Zn-air batteries. *Energy Environ Sci*. **2018**, 11(7), 1723-1729. DOI:10.1039/c8ee00977e

23. Yoo E, Zhou H. Fe phthalocyanine supported by graphene nanosheet as catalyst in Li-air battery with the hybrid electrolyte. *J Power Sources*. **2013**, 244, 429-434. DOI:10.1016/j.jpowsour.2012.11.132
24. Zhao Y, Ding Y, Song J, et al. Sustainable Electrical Energy Storage through the Ferrocene/Ferrocenium Redox Reaction in Aprotic Electrolyte. *Angewandte Chemie International Edition*. **2014**, 53(41), 11036-11040. DOI:10.1002/ANIE.201406135
25. Etsè KS, Boschini F, Karegeya C, et al. Exploring organo-palladium(II) complexes as novel organometallic materials for Li-ion batteries. *Electrochim Acta*. **2020**, 337. DOI:10.1016/j.electacta.2020.135659
26. Roex E, Etsè KS, Cloots R, Boschini F, Mahmoud A. Improving the electrochemical performances of organo-palladium (II) complex as promising anode material for Li-ion batteries: Effect of double emulsion preparation. *J Power Sources*. **2021**, 496. DOI:10.1016/j.jpowsour.2021.229827
27. Zhang J, Richardson HW. Copper Compounds. *Ullmann's Encyclopedia of Industrial Chemistry*. Wiley-VCH Verlag GmbH & Co. KGaA, **2016**, 1-31. DOI:10.1002/14356007.a07_567.pub2
28. Akkerman QA, Manna L. What Defines a Halide Perovskite? *ACS Energy Lett*. **2020**, 5(2) 604-610. DOI:10.1021/acsenergylett.0c00039
29. Widmann A, Kahlert H, Petrovic-Prelevic I, et al. Structure, insertion electrochemistry, and magnetic properties of a new type of substitutional solid solutions of copper, nickel, and iron hexacyanoferrates/hexacyanocobaltates. *Inorg Chem*. **2002**, 41(22), 5706-5715. doi:10.1021/ic0201654
30. Moonla C, Jankhunthod S, Ngamchuea K. Copper Hexacyanoferrate as a Novel Electrode Material in Electrochemical Detection of Cumene Hydroperoxide. *J Electrochem Soc*. **2021**, 168(11), 116507. DOI:10.1149/1945-7111/ac3780
31. Piernas Muñoz MJ, Castillo Martínez E. Prussian blue and its analogues. Structure, characterization and applications. *SpringerBriefs in Applied Sciences and Technology*. **2018**, 9-22. DOI:10.1007/978-3-319-91488-6_2
32. Pietro Miscione G, Angels Carvajal M, Bottoni A, Novoa J, Pietro G, Novoa JJ. A Theoretical Investigation on the Oxidation States of Palladium Complexes and their Role in Carbonylation Reaction. *Mol Phys*. **2010**, 108(12), 1619-1640. DOI:10.1080/00268976.2010.486139ï
33. Crabtree RH. The Organometallic Chemistry of the Transition Metals, John Wiley & Sons, Inc. **2014**, 163-185. DOI: 10.1002/9781118788301.ch6
34. Casado AL, Espinet P. On the Configuration Resulting from Oxidative Addition of RX to $Pd(PPh_3)_4$ and the Mechanism of the Cis-to-Trans Isomerization of $[PdRX(PPh_3)_2]$

Complexes (R=Aryl, X=Halide). *Organometallics.* **1998**, 17(5) 954–959. DOI:10.1021/om9709502

35. Vicente J, Abad JA, Frankland AD, Ramírez De Arellano MC. Synthesis and Reactivity of 2-Aminophenylpalladium(II) Complexes: Insertion Reactions of Oxygen and Carbon Monoxide into Carbon-Palladium Bonds-New Examples of “Transphobia.” *Chem-Eu J.* **1999**, 5(10), 3066-3075. DOI:10.1002/(SICI)1521-3765(19991001)5:10<3066::AID-CHEM3066>3.0.CO;2-F

Webpages

3. España es el segundo país europeo que más energía eléctrica generó con eólica y solar en 2021 | Red Eléctrica. (accessed December 8, 2022). https://www.ree.es/es/sala-de-prensa/actualidad/nota-de-prensa/2022/06/espana-es-el-segundo-pais-europeo-que-mas-energia-electrica-genero-con-eolica-y-solar-en-2021

9. SUPPORTING INFORMATION

9.1. Visuals of the experimental part

Photographs taken during the synthesis of the target complexes:

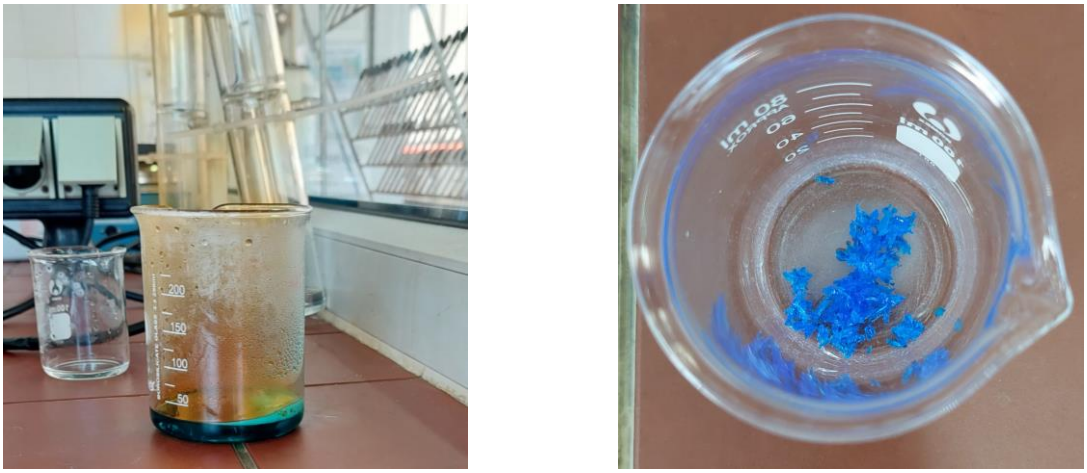

Figure S1. *NO_2 evolution in the synthesis of $Cu(NO_3)_2$ (left) and isolated $Cu(NO_3)_2 \cdot 3H_2O$ crystals (right).*

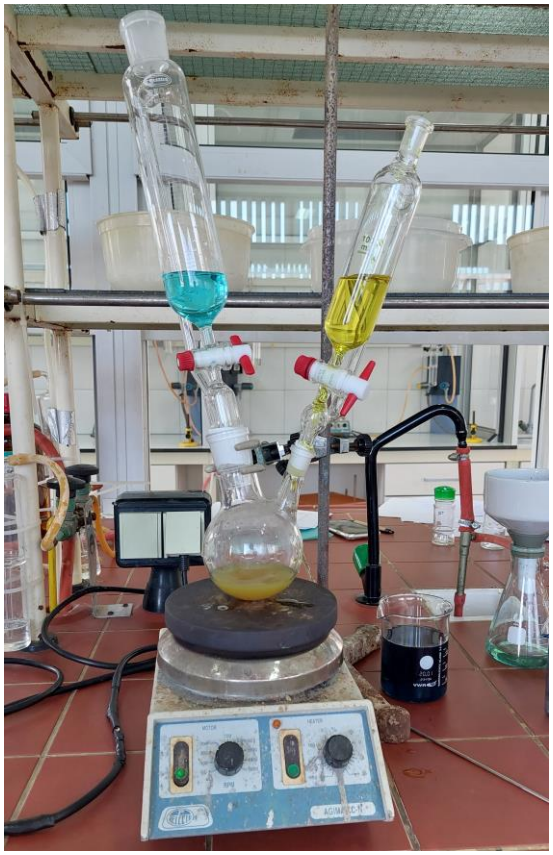

Figure S2. *Experimental setup for the synthesis of CuHCF and Prussian Blue (the photo corresponds to the CuHCF example).*

Figure S3. *Prussian Blue (**PB**) (top) and CuHCF (**A**) (bottom) suspensions before and after leaving them to settle overnight.*

Figure S4. *Reaction crude during the synthesis of [PdI{(C_6H_4)-4-NH_2}(PPh_3)$_2$] (**C**) (left) and suspension formed during the washing procedure (right).*

Figure S5. *Prussian Blue (**PB**) (left), CuHCF (**A**) (centre) and [PdI{(C_6H_4)-4-NH_2}(PPh_3)$_2$] (**C**) (right) solids after drying.*

9.2. Labware and other equipment

2 x 250 mL beakers, 2 x 50 mL beakers

1 x 100mL volumetric cylinder

2 x 50 mL volumetric flasks

2 x two-necked round bottom flasks

3 x pressure equalizing dropping funnels

4 x stirring magnets

2 x stirring plates

2 x Büchner funnels and flasks

Ultrasonic bath

Clamps and stands

Balance

2 x watch glasses

4 x glass Pasteur pipettes and bulbs

1 x 1 mL pipette, 1 x 5 mL pipette, 1 x 25 mL pipette

Pipette sucker

2 x mortar and pestle

1 x glass funnel

Filter paper

3 x plastic vials

2 x spatulas

2 x silicon stoppers

4 x centrifugation tubes

1 x 50 mL Schlenk

2 x glass vials

1 x 20 mL glass syringe

9.3. Reagents and solvents safety data

Copper — Not hazardous.

Nitric acid (65%) — May intensify fire; oxidizer. May be corrosive to metals. Causes severe skin burns and eye damage. Toxic if inhaled. Keep away from heat, hot surfaces, sparks, open flames and other ignition sources. Keep away from clothing and other combustible materials. Wear protective gloves/ protective clothing/ eye protection/ face protection. Corrosive to the respiratory tract.

Potassium Hexacyanoferrate (III)

Causes serious eye irritation. Toxic to aquatic life with long lasting effects. Wash skin thoroughly after handling. Avoid release to the environment. Wear eye protection/ face protection. Collect spillage.

Iron (III) nitrate nonahydrate

Causes severe skin burns and eye damage. Do not breathe dust. Wear protective gloves/ protective clothing/ eye protection/ face protection. Wash contaminated clothing before reuse.

Potassium Hexacyanoferrate (II) trihydrate

Harmful to aquatic life with long lasting effects. Avoid release to the environment. Contact with acids liberates very toxic gas.

4-iodoaniline — Harmful is swallowed. Causes skin irritation. Causes serious eye irritation. May cause respiratory irritation. Avoid breathing dust. Wash skin thoroughly after handling. Do not eat, drink or smoke when using this product.

Tetrakis(triphenylphosphine) palladium (0)

Harmful if swallowed. Wash skin thoroughly after handling. Do not eat, drink, or smoke when using this product. Dispose of contents/container to an approved waste disposal plant.

Toluene — Highly flammable liquid and vapor. May be fatal if swallowed and enters airways. Causes skin irritation. May cause drowsiness or dizziness. Suspected of damaging the unborn child. May cause

	damage to organs through prolonged or repeated exposure. Harmful to aquatic life with long lasting effects. Keep away from heat, hot surfaces, sparks, open flames, and other ignition sources. Avoid release to the environment.
Hexane	Highly flammable liquid and vapor. May be fatal if swallowed and enters airways. Causes skin irritation. May cause drowsiness or dizziness. Suspected of damaging fertility. May cause damage to organs through prolonged or repeated exposure if inhaled. Toxic to aquatic life with long lasting effects. Keep away from heat, hot surfaces, sparks, open flames, and other ignition sources. Avoid release to the environment.

9.4. NMR spectra related to the synthesis of C

NMR spectra for the reagents:

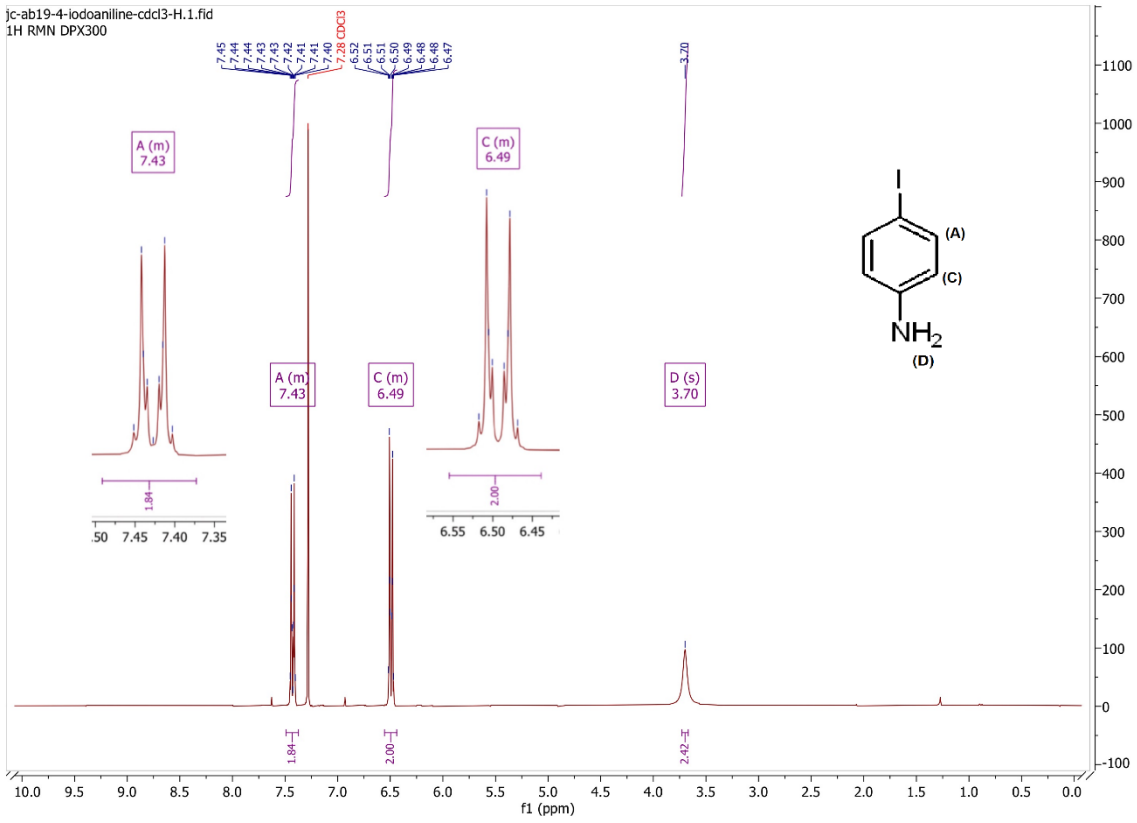

Figure S6. *^{1}H NMR spectrum of 4-iodoaniline in $CDCl_3$, with ampliations of the A and C peaks.*

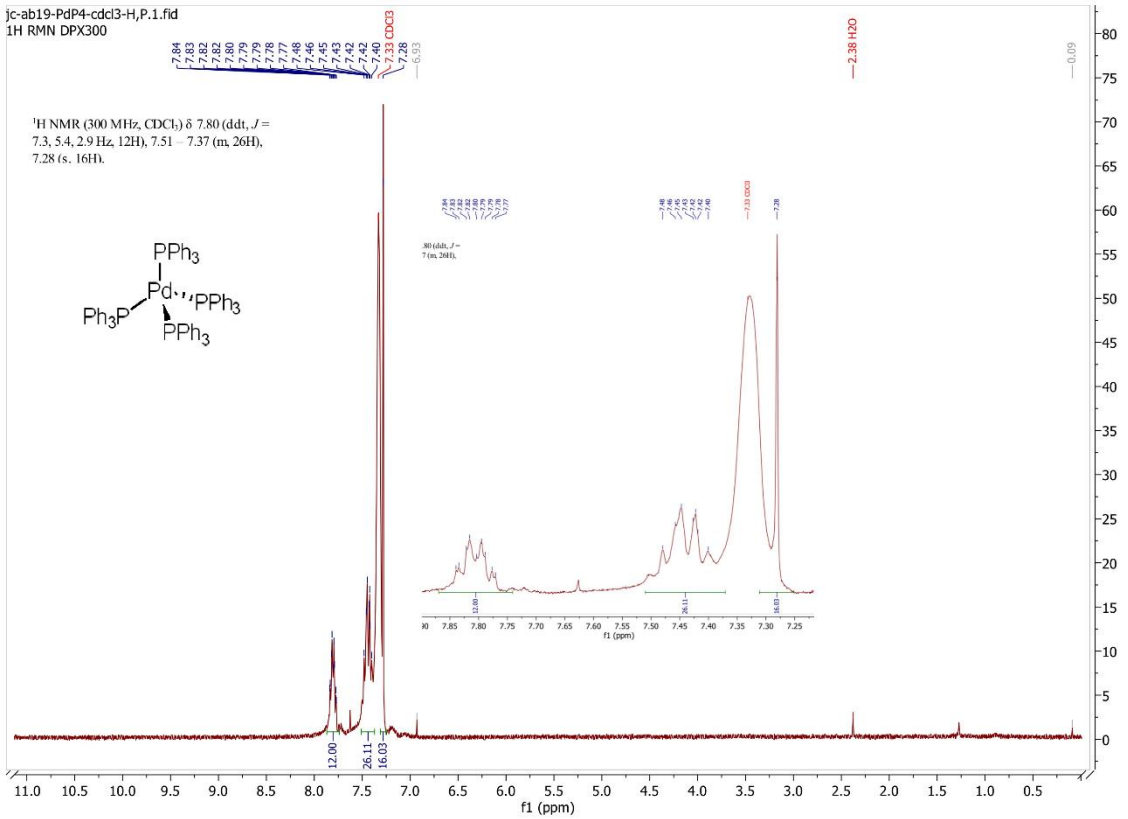

Figure S7. *^{1}H NMR spectrum of [Pd(PPh$_3$)$_4$] in CDCl$_3$, with an ampliation of the aromatic region.*

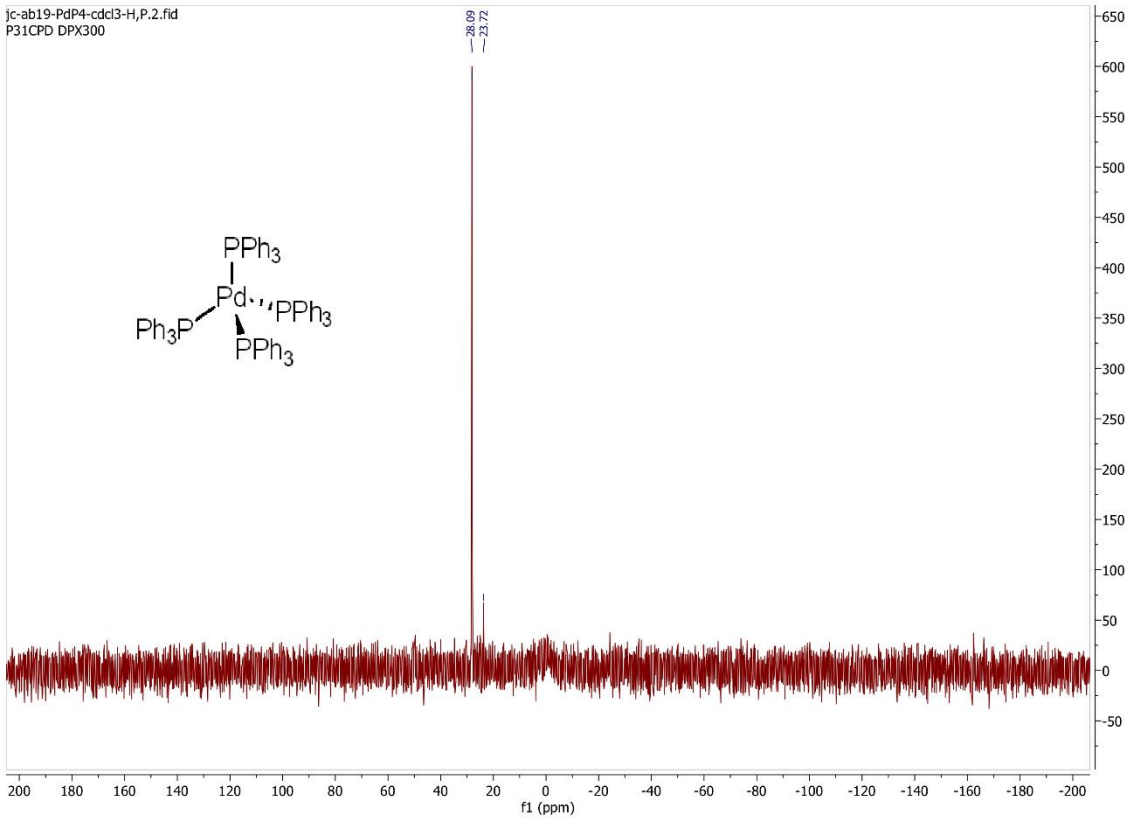

Figure S8. *^{31}P{^{1}H} NMR spectrum in in CDCl$_3$ of [Pd(PPh$_3$)$_4$].*

NMR spectra related to the reaction monitoring after one hour:

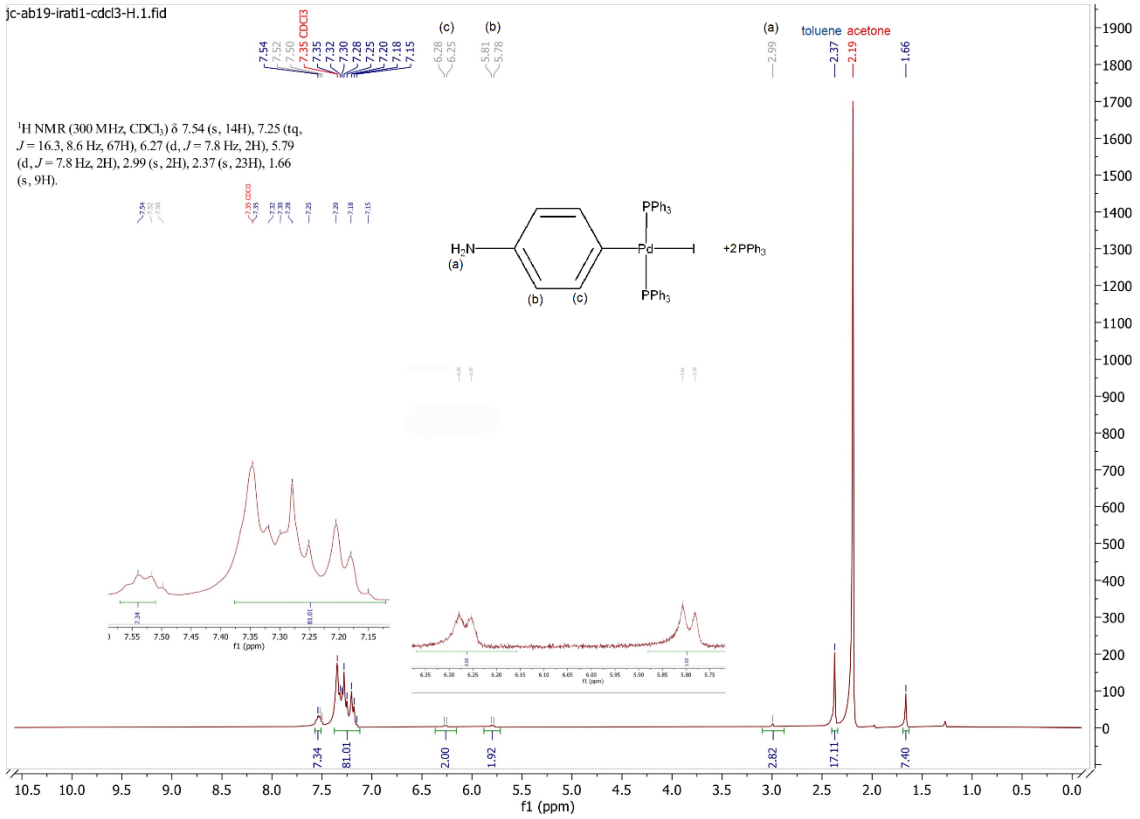

Figure S9. *^{1}H NMR spectrum in $CDCl_3$ of an aliquot of the reaction crude, with ampliations of the most deshielded peaks.*

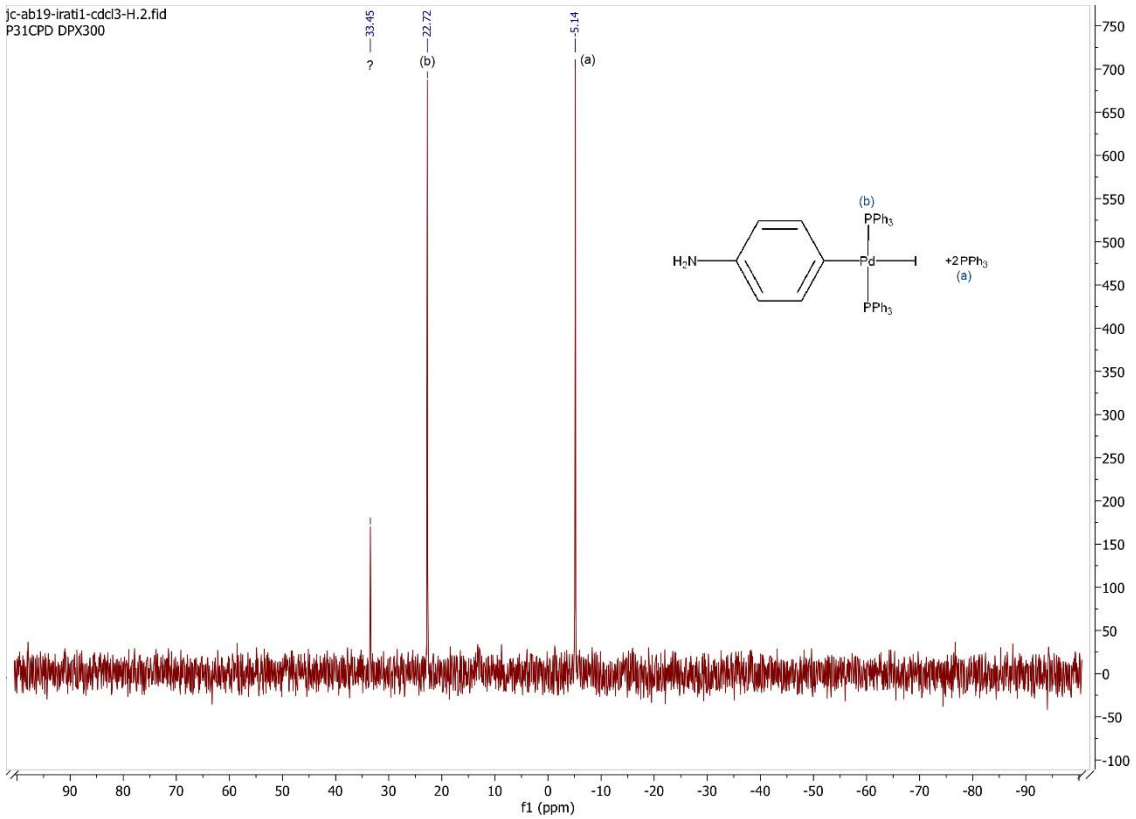

Figure S10. *$^{31}P\{^{1}H\}$ NMR spectrum in $CDCl_3$ of an aliquot of the reaction crude.*